

Article

Bimetallic Assembled Silver Nanoparticles Impregnated in *Aspergillus fumigatus* Extract Damage the Bacterial Membrane Surface and Release Cellular Contents

Saddam Saqib ^{1,2,3,†} , Saima Faryad ^{1,†}, Muhammad Irfan Afridi ^{1,4} , Bushra Arshad ^{1,5}, Muhammad Younas ¹, Muhammad Naeem ⁶ , Wajid Zaman ^{7,*} , Fazal Ullah ⁸ , Momina Nisar ¹, Sajid Ali ^{9,*} , Abdallah M. Elgorban ¹⁰ , Asad Syed ¹⁰, Hosam O. Elansary ¹¹  and Tarek K. Zin El-Abedin ¹²

- ¹ Department of Biotechnology, Mohi-Ud-Din Islamic University, Nerian Sharif 12080, AJ&K, Pakistan
 - ² University of Chinese Academy of Sciences, Beijing 100049, China
 - ³ State Key Laboratory of Systematic and Evolutionary Botany, Institute of Botany, Chinese Academy of Sciences, Beijing 100093, China
 - ⁴ State Key Laboratory of Chemo/Biosensing and Chemometrics, College of Biology, Hunan University, Changsha 410012, China
 - ⁵ Pakistan Council for Science and Technology, Ministry of Science and Technology, Islamabad 44000, Pakistan
 - ⁶ China Sinovita Bioengineering Group, Jinan 250000, China
 - ⁷ Department of Life Sciences, Yeungnam University, Gyeongsan 38541, Korea
 - ⁸ State Key Laboratory of Grassland Agro-Ecosystems, School of Life Sciences, Lanzhou University, Lanzhou 730000, China
 - ⁹ Department of Horticulture and Life Science, Yeungnam University, Gyeongsan 38541, Korea
 - ¹⁰ Botany and Microbiology Department College of Science, King Saud University, P.O. Box 2455, Riyadh 11451, Saudi Arabia
 - ¹¹ Plant Production Department, College of Food & Agriculture Sciences, King Saud University, Riyadh 11451, Saudi Arabia
 - ¹² Department of Agriculture & Biosystems Engineering, Faculty of Agriculture (El-Shatby), Alexandria University, Alexandria 21545, Egypt
- * Correspondence: shangla123@gmail.com (W.Z.); drsajid@yu.ac.kr (S.A.)
 † These authors contributed equally to this work.



Citation: Saqib, S.; Faryad, S.; Afridi, M.I.; Arshad, B.; Younas, M.; Naeem, M.; Zaman, W.; Ullah, F.; Nisar, M.; Ali, S.; et al. Bimetallic Assembled Silver Nanoparticles Impregnated in *Aspergillus fumigatus* Extract Damage the Bacterial Membrane Surface and Release Cellular Contents. *Coatings* **2022**, *12*, 1505. <https://doi.org/10.3390/coatings12101505>

Academic Editors: Giuseppe Cirillo and Anton Fikai

Received: 16 September 2022

Accepted: 5 October 2022

Published: 9 October 2022

Publisher's Note: MDPI stays neutral with regard to jurisdictional claims in published maps and institutional affiliations.



Copyright: © 2022 by the authors. Licensee MDPI, Basel, Switzerland. This article is an open access article distributed under the terms and conditions of the Creative Commons Attribution (CC BY) license (<https://creativecommons.org/licenses/by/4.0/>).

Abstract: The bactericidal effects of nanomaterials play an essential role in cytoplasmic leakage, leading to bacterial cell death. In this study, silver nanoparticles (AgNPs) were synthesized using a fungal extract of *Aspergillus fumigatus* (*A. fumigatus*). The physicochemical properties of the bare and myco-synthesized AgNPs (MS-AgNPs) were examined by X-ray diffraction (XRD), Fourier transform infrared (FT-IR) spectroscopy, ultraviolet–visible (UV–vis) spectroscopy, scanning electron microscopy (SEM), energy dispersive X-ray spectroscopy (EDX), and transmission electron microscopy (TEM). XRD revealed the crystalline structure of the prepared NPs. The FTIR spectrum of the MS-AgNPs revealed the presence of the stretching vibrations of hydroxyl (–OH) and carbonyl groups (C=O). The UV results showed absorption from 450 nm to 590 nm, confirming the synthesis of the AgNPs. SEM and TEM showed rough cubic shapes (spheres), 20–60 nm in size, while EDX confirmed the presence of 60% Ag in the sample. The MS-AgNPs revealed the highest antibacterial activity against *Staphylococcus aureus*, with a zone of inhibition of 18.21 ± 2.1 mm, followed by *Shigella dysenteriae* and *Salmonella typhi*. The bimetallic-AgNPs played a vital role in cell membrane damage and the release of cellular contents, specifically nucleic acids and proteins. These results suggest that MS-AgNPs have promising antimicrobial capabilities and might be beneficial for an extensive array of biological applications.

Keywords: antibacterial; bimetallic; cell membrane; cellular contents; nanomaterials; myco-synthesized AgNPs

1. Introduction

The microbial resistance of pathogenic microorganisms against antibiotics has highlighted the need for replacements (such as metallic nanoparticles) to overcome this issue [1,2]. Therefore, the development of novel operational antimicrobials becomes indispensable. Metal nanoparticles have numerous exclusive physicochemical characteristics that are remarkably different and beneficial compared to the bulk material, making them potent candidates in biomedical applications [3,4]. Among them, Ag is a naturally occurring valuable metal, renowned for its resilient bactericidal activity that makes it a suitable candidate for developing bactericidal materials against pathogenic microbes [5–7]. Ag can attack multiple sites of the microbes; hence, microbes must develop a set of mutations to counterbalance themselves [8,9]. This quality of Ag makes it virtually impossible for pathogens to develop resistance against pathogenic bacteria and fungi [10]. Moreover, the AgNPs capped with the therapeutic metabolites of plants, algae, endophytic bacteria, and fungi interact with the bacterial cell membrane, causing the leakage of proteins and cellular content, ultimately leading to bacterial cell death [11,12].

The manufacture of NPs from biological resources, such as plant extracts, fungal metabolites, and bacterial filtrates, further improves the applications of NPs [13–16]. Living organisms maintain distinctive auspicious characteristics to engineer nanomaterials with pre-determined applications [17,18]. MS-AgNPs are innovative and more suitable for large-scale industrial manufacturing because of their substantial growing speed, modest culturing techniques, huge secretion quantity of extracellular enzymes, enhanced capability of better survival with nanoparticles (ensure protein coating), and outstanding cohesion with a nanoparticle-rich environment [19,20]. Microorganisms, such as yeast, endophytic bacterial strains, and fungal strains, possessing medicinal metabolites serve as micro-factories for the biogenic synthesis of nanoparticles [21–23]. The fungal metabolites, polymers, and polypeptides facilitate the binding and reduction of metal salts to NPs. Previous studies showed that metal nanoparticles, including gold, silver, iron, platinum, zinc, and cobalt, can be manufactured with fungi and its metabolites due to their mycelia and secondary metabolites, representing an enormous surface area for communication [24–26]. The biosynthesized NPs functionalized with organic metabolites, such as carboxylate and amines groups, aid in the bioconjugation of NPs on inert supports for heterogeneous biological activities [27,28]. Therefore, utilizing endophytic fungi is an easy and cost-effective approach for transforming metal salts into metal nanoparticles.

Previous studies reported the biosynthesis of AgNPs with the *Aspergillus* family, including *A. terreus*, *A. fumigatus*, *A. oryzae*, *A. niger*, *A. flavus*, *A. clavatus*, and *A. conicus* [29–31]. These fungal strains possess efficient mechanisms for secreting extracellular enzymes, which help in the synthesis process by reducing the enzymes extracellularly or intracellularly [32,33]. Among these, *A. fumigatus* showed the remarkable capability of manufacturing AgNPs by reducing enzymes in a short time [34,35]. *A. fumigatus* is an endophytic fungus that can induce noninfectious cohesion with healthy plants [36,37]. The fungal-mediated synthesis and antibacterial potential of AgNPs have been reported in numerous studies [38,39]. On the other hand, this study assesses the catalytic potential of *A. fumigatus* in manufacturing AgNPs, as well as their bactericidal effect. In this study, a facile and eco-friendly method was developed to synthesize AgNPs by mediating *A. fumigatus*. The roles of *A. fumigatus* and the physiochemical properties of the MS-AgNPs were examined by X-ray diffraction (XRD), Fourier transform infrared (FT-IR) spectroscopy, ultraviolet-visible (UV-vis) spectroscopy, scanning electron microscopy (SEM), energy dispersive X-ray spectroscopy (EDX), and transmission electron microscopy (TEM). In addition, the role of MS-AgNPs in bacterial cell membrane damage and the release of cellular contents, specifically nucleic acids and proteins, were evaluated. The results revealed changes in the bacterial cell membrane surface after treatment with the NPs due to the release of cellular contents, which leads to bacterial membrane damage and cell death.

2. Materials and Methods

2.1. Chemical Reagents

Sodium chloride (NaCl), tryptone, ethanol (CH₃CH₂OH), silver nitrate (AgNO₃), agar-agar, Mueller–Hinton agar, potassium dihydrogen phosphate (KH₂PO₄), Magnesium sulfate heptahydrate (MgSO₄ · 7H₂O), ammonium sulfate (NH₄)₂SO₄, glucose, acetone (C₃H₆O), and potato dextrose agar media (PDA) were purchased from Sigma–Aldrich (Burlington, VT, USA). *A. fumigatus* was obtained from Quaid-i-Azam University, Islamabad, Pakistan. Milli-Q water was used in all experiments.

2.2. Extracellular Mycogenic AgNPs Synthesis

The fungus was cultivated on fresh PDA media to obtain a pure culture. The fresh culture of *A. fumigatus* was cultured in an Erlenmeyer flask possessing 100 mL of potato dextrose broth (PDB) at 32 °C with shaking on an orbital shaker for 4 days at 100 rpm to collect the biomass. A sterile plastic sieve was used to collect the fungal biomass. The mycelium was washed with sterile distilled water to remove the remnants and debris. The mycelium was mixed with 200 mL ultrapure water and stirred for 48 h at 30 °C. The culture was filtered through Whatman paper, and the filtrate was used for the myco-synthesis of nanoparticles. Subsequently, the supernatant was mixed with 50 mL of a 1 mM AgNO₃ suspension and stirred in the dark at 30 °C with 50 mL of cell filtrate for 48 h to prepare the AgNPs [9]. The reaction mixture was centrifuged at 12,000 rpm at 4 °C. The supernatant was removed while the pellet containing nanoparticles was washed three times with distilled water. The prepared nanoparticles were oven dried to remove the water and stored for further use. The bare AgNPs were synthesized using the following chemical reduction method [40]. Briefly, 50 mL of a 1 × 10^{−3} M AgNO₃ solution in double distilled water was heated on a hot plate. Subsequently, 5 mL (1%) of trisodium was added dropwise. The solution was mixed with a magnetic stirrer at 80 rpm and heated until the solution color changed to dark brown. The solution was centrifuged at 12,000 rpm to remove the supernatant, and the pellet was dried and calcined for further use.

2.3. UV-vis absorbance spectroscopy

The color change in the biosynthesized AgNPs was observed visually, while the synthesis was confirmed using a UV-vis spectrophotometer (Dynamical Limited, Sydney, Australia) at 1 nm resolution between 200 to 800 nm with 1856 nm/min scanning speed.

2.4. Assessment of the XRD Pattern

The XRD patterns were obtained on a PAN analytical X'pert PRO X-ray diffractometer (JEOL, Tokyo, Japan) in the range of 20–80° 2θ with a current of 40 mA fixed at 45 kV. The sample was processed with a drop coating of myogenic AgNPs suspension on a glass substrate. The average crystal size was measured using Scherrer's equation ($D = K \lambda / \beta \cos \theta$), where D shows the size of the Ag NPs; λ indicates the wavelength (1.540); β is the full width at half maximum of the diffraction peak (FWHM); K is the Scherrer's constant; and θ is the Bragg's angle.

2.5. SEM, EDX, and TEM Analysis

The morphology and composition of MS-AgNPs impregnated in *A. fumigatus* extract and bare AgNPs were examined by SEM (Model, JSM5910, JEOL, Tokyo, Japan) associated with EDX (JSM5910, JEOL, Tokyo, Japan). Sample preparation was performed using the reported protocol [11]. Twenty-four hours after adding AgNO₃, the SEM slides were prepared from a smear of the AgNPs. The sample was then coated with a thin gold–palladium layer to make it conductive. SEM was set at an accelerating voltage of 20 kV upon gold coating for 4 min. The samples were visualized by SEM at the CRL (Central Resource Laboratory, Model, JSM5910, JEOL, Tokyo, Japan) University of Peshawar, Pakistan. Polaroid P/N 665 film was used to obtain the micrographs.

An EDX spectrometer was used to determine the elemental composition of the samples. The particle structure and particle size distribution were evaluated by TEM (Model, JEM-2100, JEOL, Tokyo, Japan).

2.6. Antimicrobial Activity of Silver Nanoparticles

The MS-AgNPs impregnated in the *A. fumigatus* extract were analyzed for their antibacterial activity using a well diffusion assay, and the optical density of the liquid broth was measured to examine bacterial growth.

2.6.1. Agar Well Diffusion Method

The standard agar well diffusion method was used to assess the antibacterial assay of the prepared AgNPs solution. The purified cultures of the selected pathogenic bacterial strains (*S. aureus*, *S. dysenteriae*, and *S. typhi*) were re-cultured using nutrient agar plates for 24 h at 32 ± 2 °C. The prepared agar plates were streaked with the pure pathogenic bacterial strains at 10^4 colony-forming units (CFU/mL) separately using aseptic cotton swabs. The 5 mm diameter wells were made with a cork borer inside the gel. After solidification of the agar, 10 µL saline solution of bacterial strain was infused on a nutrient agar plates in each well. Subsequently, a micropipette was used to load 30 µL of the MS-AgNPs (3 mM concentration). The same amount of the chemically synthesized NPs (bare AgNPs) was also used to compare the results. In addition, an antibiotic (ampicillin, 3 mM concentration) was used as a positive control, while distilled water of the same volume was used as a negative control [41]. All plates were incubated at 37 °C for 16 h to check the inhibition zones. The test was conducted in triplicate, and the inhibition zones were recorded using a scale.

2.6.2. Growth Curve Assay

The antibacterial potential of the liquid medium was assessed by evaluating the growth inhibition of selected pathogenic bacteria (*S. aureus*, *S. dysenteriae*, and *S. typhi*) by measuring the optical density (OD) using a UV–visible spectrophotometer (Agilent-9453, Wilmington, NC, USA) after 8, 16 and 24 h. Microbe-free liquid broth was prepared according to standard procedures and kept for cooling under a sterile environment in a laminar flow. Liquid broth (15 mL) was poured into each test tube separately. Later, 50 µL prepared bacterial cultures with 3 mM MS-AgNPs were added. Bare-AgNPs were used for comparison. An antibiotic (ampicillin) was applied as a positive control, whereas distilled water was used as the negative control. Pathogenic bacterial strains including *S. aureus*, *S. dysenteriae*, and *S. typhi* were inoculated in three different test tubes. These test tubes were then covered with cotton plugs and incubated in Mueller–Hinton liquid medium (broth) at 37 °C overnight. After different time intervals (8, 16, and 24 h) the absorbance was measured using a UV spectrophotometer.

2.7. Bacterial Cell Surface Potential

The cell membrane integrity was analyzed before and after treatment with the bare and MS-AgNPs by recording the cell surface charge utilizing a zeta potential analyzer. The bacterial cells were centrifuged at 12,000 rpm for 10 min to harvest bacterial cells from the supernatant. The bacterial cells were resuspended in phosphate-buffered saline (PBS) of 0.06 molar (M) concentration and 7.4 pH, to treat the NPs. The cells (1×10^6) were treated with MS-AgNPs, bare AgNPs, and an antibiotic (ampicillin), and MS-AgNPs in the absence of bacterial cell was used as control. The same concentration (3mM) was used for all the treatments (MS-AgNPs, bare AgNPs, and ampicillin). The treated cells were incubated in a shaker incubator at 38 °C for 4 h at 150 rpm. The zeta potential values of the treated and control samples were measured using a zeta potential analyzer at 280 nm.

2.8. Cell Constituents Release

The potential of the MS-AgNPs was determined by analyzing the cell constituents discharged in the media. The cells were treated with bare and MS-AgNPs, antibiotic (ampicillin), and control (distilled water). The cells were stored at 38 °C for 4 h. The incubated cells were isolated by centrifugation for 10 min at 12,000. The cell constituent release was determined by measuring the absorbance of the supernatant at 260 nm.

3. Results

3.1. Myco-synthesis of AgNPs

The myco-synthesis of AgNPs impregnated in *A. fumigatus* extract was performed, and its antibacterial potential against pathogenic bacteria was assessed. Hence, the selected fungal strain showed excellent ability for the biosynthesis of AgNPs. The co-precipitate method was used to prepare the impregnated nano-sized AgNPs in the fungal extract of *A. fumigatus* and approved by the color change within the reaction mixture. The light brown filtrate of *A. fumigatus* was incubated with the nano-sized Ag particle, and this mixture changed into a brownish color when the reaction was complete (Figure 1), in the case of MS-AgNPs. The bare AgNPs showed a light brownish appearance. Similar results are also reported by [41].

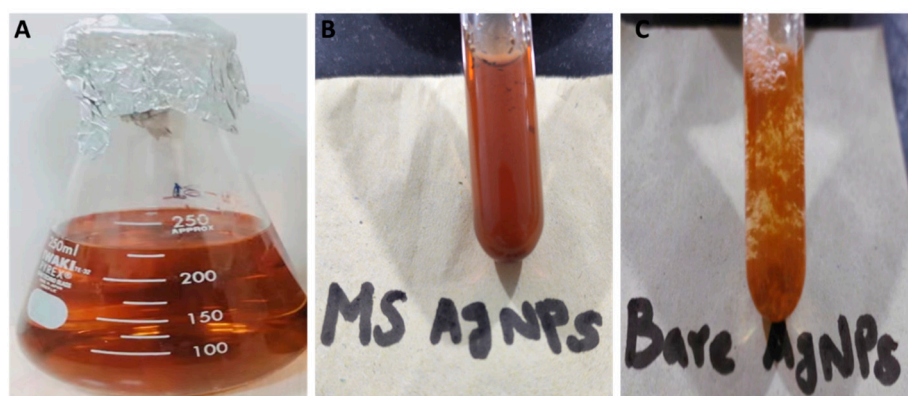


Figure 1. Visual appearance of MS-AgNPs and bare AgNPs; (A) fungal filtrate, (B) MS-AgNPs, and (C) bare AgNPs.

3.2. Characterization of the Myco-synthesized Silver Nanoparticles (AgNPs)

3.2.1. XRD

XRD was used to examine the crystallinity of the MS-AgNPs and bare AgNPs. The prepared AgNPs were crystalline. The XRD patterns of the MS-AgNPs revealed six characteristic peaks at 34.3°, 36.2°, 39.4°, 48.1°, 52.5°, and 78.4° 2 θ , which were assigned to the (210), (311), (220), (111), (420), and (110) planes, respectively (Figure 2, black spectrum). XRD revealed the face-centered cubic (fcc) structure of Ag, which is in accordance with the powder diffraction standards (JCPDS) card no. 89-3722, revealing the lattice parameter $a = 3.07$ Å. The unknown peaks observed in the black spectrum of the MS-AgNPs (represented by asterisks) may be due to the presence of organic metabolites of the fungal extract [42]. The XRD pattern of both bare AgNPs and MS-AgNPs showed that Ag is the major element of the composite. By contrast, the bare AgNPs showed the same XRD peaks, with little deviation. The bare AgNPs revealed six peaks at 18.1°, 28.4°, 31.6°, 39.7°, 41.7°, and 49.1° 2 θ , which were assigned to the (121), (111), (412), (333), (210), and (114) planes, respectively (Figure 2, red spectrum). The peaks for the bare-AgNPs are in agreement with JCPDS file no. 42-0783, with a lattice parameter of 2.08 Å. The mean crystallite sizes of the MS-AgNPs and bare AgNPs were 39 nm and 41 nm, suggesting that the prepared NPs are suitable for antimicrobial applications in different fields [4,43]. The variations resulting in the diffraction pattern of XRD are due to synthesis methods, as bare AgNPs are prepared through chemical synthesis, while MS-AgNPs are prepared with the help of fungus strains.

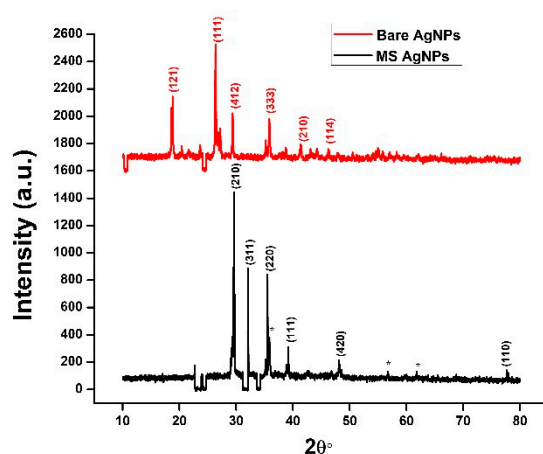


Figure 2. XRD pattern of the MS-AgNPs (black spectra) and bare AgNPs (red spectra). The * represent unknown peaks in the black spectrum.

3.2.2. FTIR

The presence of the functional groups on the surface of the MS-AgNPs was confirmed by FTIR spectroscopy. The FTIR spectrum of the MS-AgNPs revealed bands at 3423.76 cm^{-1} and 3316.35 cm^{-1} analogous to the hydroxyl ($-\text{OH}$) stretch coupled with a carbonyl group ($\text{C}=\text{O}$). The absorbances at 3018.90 cm^{-1} and 2365.62 cm^{-1} were attributed to the $\text{C}-\text{H}$ and $\text{N}-\text{H}$ stretching, respectively. The peaks at 1730.79 cm^{-1} and 1630.51 cm^{-1} confirmed the presence of the NH_2 stretching vibration of a carbonyl and the $\text{C}=\text{C}$ stretching of alkenes, respectively. A sharp peak at 1394.28 cm^{-1} showed $\text{C}-\text{N}$ stretching. By contrast, the peaks at 997.98 cm^{-1} and 913.42 cm^{-1} were reciprocal to the alcohol OH band and CO carboxylic anions, respectively. In addition, the peak observed at 529.36 cm^{-1} was attributed to the $\text{C}-\text{N}$ nitrile groups (Figure 3, black lines). By contrast, the bare AgNPs did not show peaks at 3423.76 cm^{-1} and 3316.35 cm^{-1} , demonstrating the absence of the hydroxyl ($-\text{OH}$) stretch and carbonyl group ($\text{C}=\text{O}$), respectively (Figure 3, red lines). An additional absorbance in the bare AgNPs at 1245.62 cm^{-1} indicated the presence of $-\text{NH}$ stretching modes (Figure 3, red lines). The spectrum of the bare AgNPs revealed a pattern similar to MS-AgNPs, indicating that both NPs had been synthesized.

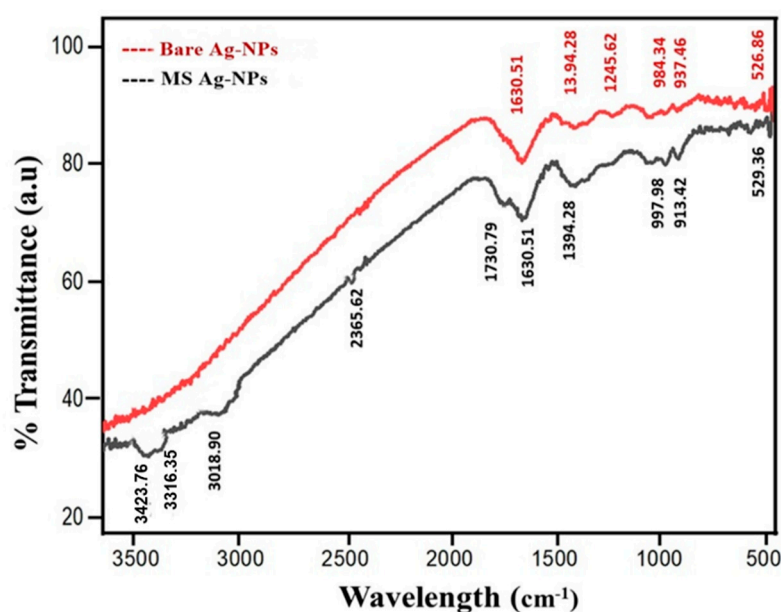


Figure 3. FTIR pattern of the bare AgNPs (red spectra) and MS-AgNPs (black spectra).

3.2.3. UV–Vis Spectroscopy

The synthesis of AgNPs was confirmed by measuring the absorbance scan at the wavelength range of 200–800 nm. UV–vis spectroscopy of both MS-AgNPs and bare AgNPs revealed a broad absorbance band from 455 nm to 534 nm, which indicate the presence of Ag^+ ions in the sample (Figure 4, red and black spectra) [44]. The appearance of a additional peaks at 506 and 535 nm may correspond to the presence of fungal metabolites (Figure 4, black spectrum) [45]. These results indicate the successful synthesis and the presence of fungal metabolites on AgNPs, which are consistent with earlier reports on the AgNPs [44,45].

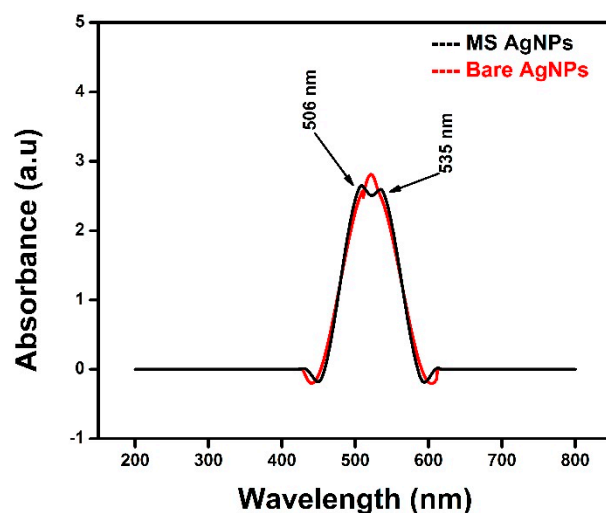


Figure 4. UV–vis spectra of bare AgNPs (red spectra) and MS-AgNPs (black spectra).

3.2.4. SEM Analysis

In discovering antimicrobial resources, it is essential to determine the morphology of MS-AgNPs and their efficacy against microbes using high-resolution microscopic techniques [46]. SEM showed NPs, with a cubic structure and a mean size ranging from 65 to 85 nm (Figure 5B). By contrast, bare AgNPs also showed a spherical structure, with a mean size ranging from 50–80 nm (Figure 5A). EDX analysis of both bare and MS-AgNPs showed the presence of more than 40% Ag and more than 25% oxygen. The presence of oxygen might have resulted from the AgNO_3 solution. MS-AgNPs groups of Na and Cl were also found, which might have resulted from fungal metabolites. Generally, the Ag-NPs revealed strong absorption peaks, which are similar to those found in previous studies [9,11]. Earlier reports showed that the existence of oxygen plays a vital role in enhancing the antimicrobial potential of AgNPs [38].

3.2.5. TEM Analysis

The TEM images of MS-AgNPs synthesized with the help of *A. fumigatus* filtrate showed that the NPs were roughly spherical (Figure 6A,B), with a particle size distribution in the range of 20–60 nm with an average size of 30 ± 6.05 nm at a magnification of $\times 50$ nm (Figure 6C,D). The NPs synthesized with the fungal extract revealed a polydispersed-like shape that might be due to the increased surface area (Figure 6A).

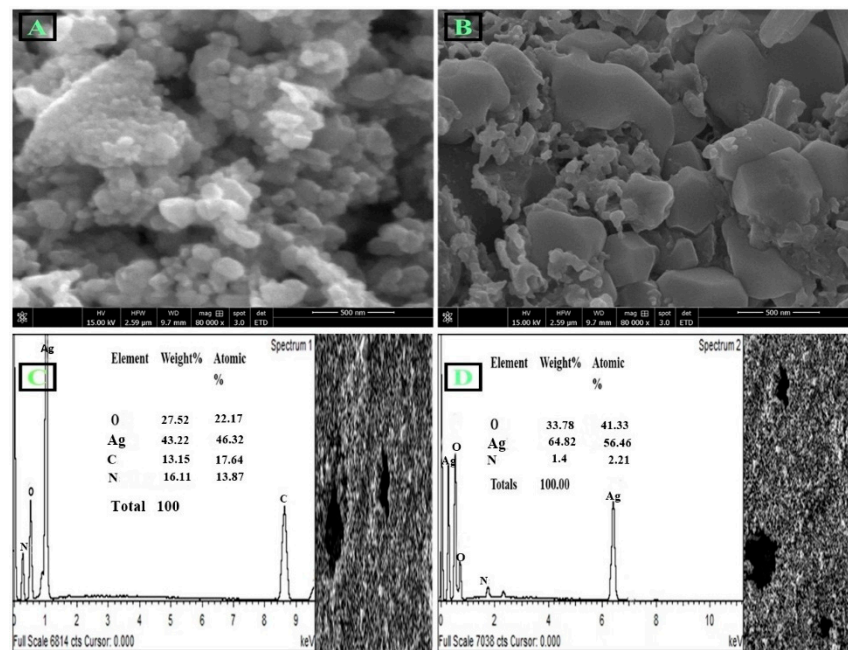


Figure 5. SEM images and EDX spectra of the synthesized AgNPs; (A) MS-AgNPs structure, (B) bare AgNPs structure, (C) MS-AgNP's EDX spectra, (D) bare AgNPs EDX spectra.

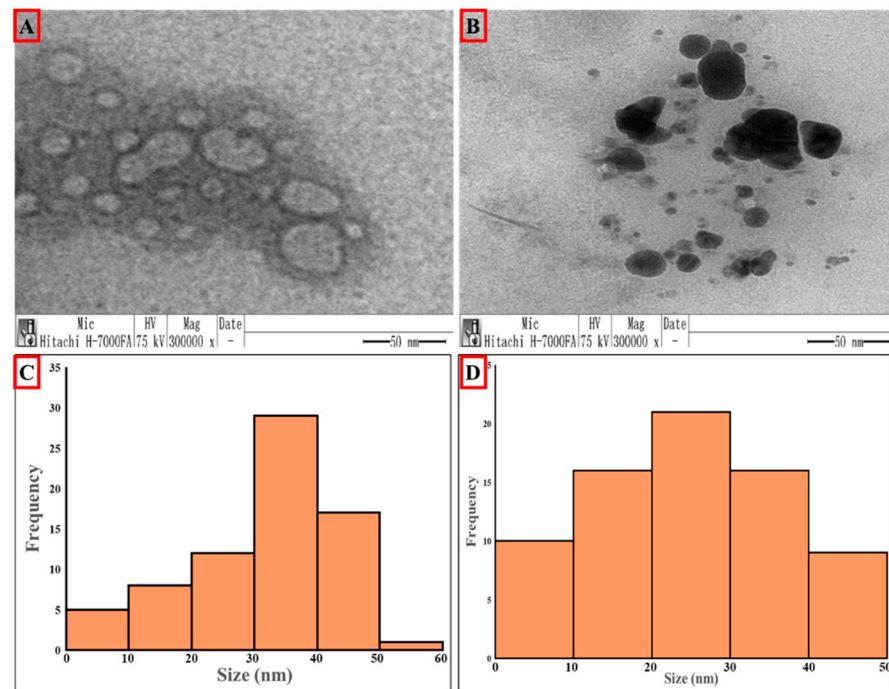


Figure 6. TEM images and particle size distribution of the synthesized AgNPs; (A) MS-AgNPs structure, (B) bare AgNPs structure, (C) MS-AgNP particle size distribution, (D) bare AgNP particle size distribution.

3.3. Antibacterial Activity

The antibacterial potential of MS-AgNPs was estimated using the agar well diffusion method to measure the zone of inhibition, and the bactericidal efficiency in liquid broth was examined from the optical density.

3.3.1. Agar Well Diffusion Method

The antibacterial potential of the MS-AgNPs and chemically synthesized bare AgNPs was evaluated against *S. aureus*, *S. dysenteriae*, and *S. typhi*. The results were presented as a zone of inhibition (Figure 7 and Table 1). The MS-AgNPs contain significant antibacterial potential against *S. aureus*, with a zone of inhibition of 18.21 ± 2.1 mm (Table 1). The MS-AgNPs were also active against *S. dysenteriae* and *S. typhi*, with a zone of inhibition of 16.18 ± 1.3 and 14.41 ± 1.7 mm, respectively. However, the bare AgNPs showed a smaller zone of inhibition (13.73 ± 1.4 , 14.84 ± 1.8 , and 13.25 ± 1.9 mm) against *S. aureus*, *S. dysenteriae*, and *S. typhi*, respectively (Table 1). Moreover, the antibiotic (ampicillin, 3 mM) as a positive control and distilled water as a negative control showed significantly smaller inhibition zones, suggesting that the MS-AgNPs have strong antibacterial potential.

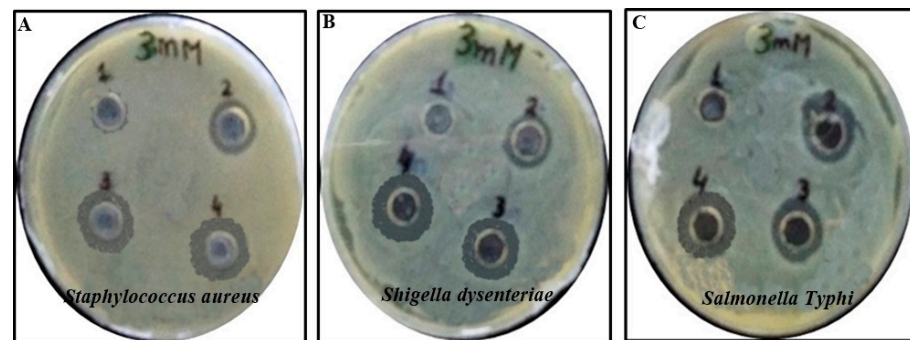


Figure 7. Antibacterial potential (zone of inhibition) of the MS-AgNPs and bare AgNPs was evaluated against (A) *S. aureus*, (B) *S. dysenteriae*, and (C) *S. typhi*; (1) control, (2) antibiotic, (3) bare AgNPs, and (4) MS-AgNPs.

Table 1. Zone of inhibition of MS-AgNPs, bare AgNPs, antibiotics, and control against pathogenic bacteria.

Treatments (3 mM) Concentration	<i>S. aureus</i>	<i>S. dysenteriae</i>	<i>S. typhi</i>
	Zone Inhibition Value (mm)	Zone Inhibition Value (mm)	Zone Inhibition Value (mm)
MS Ag-NPs	18.21 ± 2.1^a	16.18 ± 1.3^b	14.41 ± 1.7^c
Bare Ag-NPs	13.73 ± 1.4^b	14.84 ± 1.8^c	13.25 ± 1.9^{ab}
Ampicillin	7.31 ± 2.1^c	7.80 ± 1.4^d	5.51 ± 1.3^{ac}
Control	3.12 ± 1.4^d	1.15 ± 1.3^e	1.10 ± 1.4^e

Different letters indicate significant differences at $p < 0.05$ by one-way ANOVA. The values are the mean \pm SD of assessments performed in triplicate.

3.3.2. Optical Density Estimations

The optical density of the MS-AgNPs determined the death rate of the bacteria in the liquid broth at different time intervals (8, 16, and 24 h.). These results showed that MS-AgNPs actively inhibited bacterial growth of all strains at different time intervals (Figure 8). The bare AgNPs also revealed inhibition of bacterial growth, but the inhibition was slightly lower compared to that of MS-AgNPs. Maximum bacterial growth was observed in the control, followed by the antibiotic. In addition, these results also showed that the MS-AgNPs are more effective against the Gram-positive strain, which is in accordance with previous studies [47,48]. Moreover, the growth of bacterial strains increased slightly after 24 h due to cell division because at the initial stages, such as 8 h (Figure 8A) and 16 h (Figure 8B), bacterial cell division had not reached the optimum. Therefore, the inhibition up to 24 h (Figure 8C) was estimated by UV spectrophotometer.

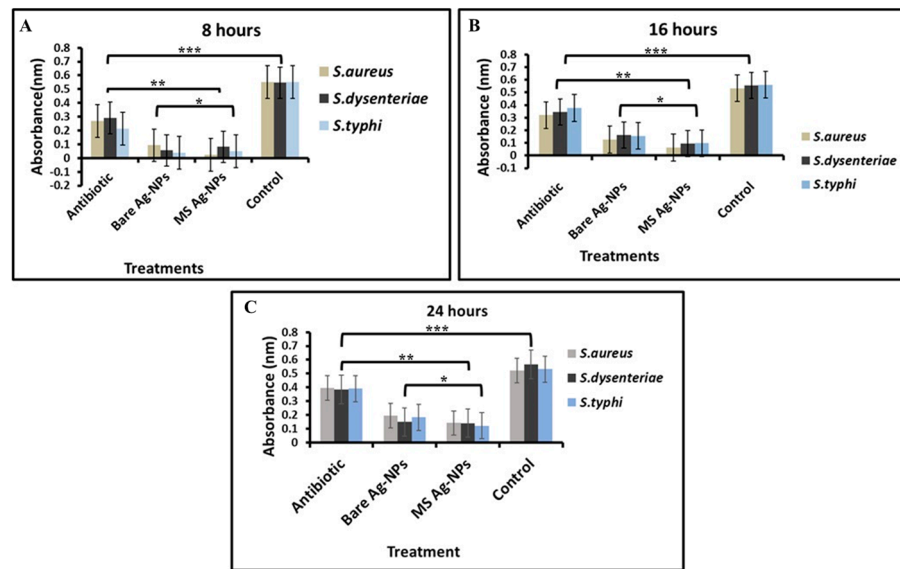


Figure 8. Optical density of the MS-AgNPs determined the growth of the bacteria in liquid broth at different time intervals (8, 16, 24 h). (A) Representative growth of the bacteria in liquid broth at 8 h, (B) representative growth of the bacteria in liquid broth at 16 h, and (C) representative growth of the bacteria in liquid broth at 24 h. Note: *** shows significant difference at $p < 0.05$, ** shows significant difference at $p < 0.01$, and * shows significant difference at $p < 0.005$.

3.4. MS-AgNP's Effect on Bacterial Membrane

The zeta potentials of the *S. aureus*, *S. dysenteriae*, and *S. typhi* were measured to examine the effect of the MS-AgNPs on the membrane surface of the bacteria. Our results showed that untreated cells of *S. aureus*, *S. dysenteriae*, and *S. typhi* revealed a zeta potential of -37 , -33 , and -29 mV, indicating a strong negative surface potential (Figure 9). The negative potential of the cells was decreased when treated with MS-AgNPs and revealed 3.6, 3.8, and 3.1 mV against *S. aureus*, *S. dysenteriae*, and *S. typhi*, respectively. Bare AgNPs also decreased the negative potential of the bacterial membrane by -3.5 , -4.3 , and -3.1 mV against *S. aureus*, *S. dysenteriae*, and *S. typhi*, respectively, whereas the control consisting of only distilled water, MS-AgNPs, bare AgNPs, and the antibiotic only revealed significant difference with treated bacterial cells. However, the negative zeta potential of the MS-AgNPs was very low as compared to other treatments, indicating that NPs exhibit the potential to affect the degradation of the membrane surface.

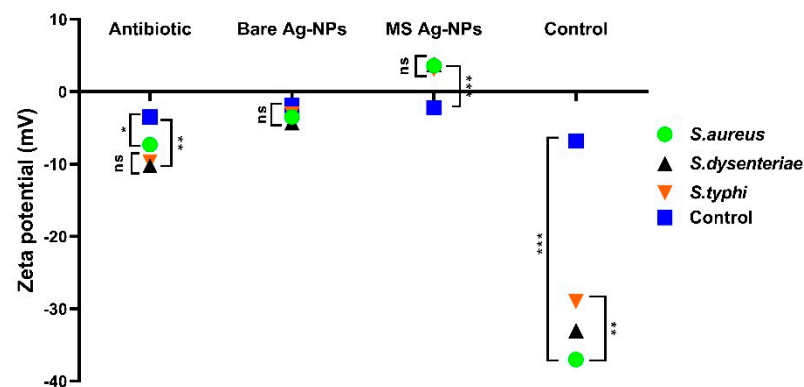


Figure 9. Zeta potential value of *S. aureus*, *S. dysenteriae*, and *S. typhi* to compare membrane surface damage caused by MS-AgNPs, Bare AgNPs, antibiotics, and control (untreated bacterial cells). Control in each treatment without bacterial cells. Control (only distilled water), control (Only MS Ag-NPs), control (only bare Ag-NPs) and control (only antibiotic). Note: *** shows significant difference at $p < 0.05$, ** shows significant difference at $p < 0.01$, and * shows significant difference at $p < 0.005$.

3.5. Analysis of Cell Constituents Release

The release of cell constituents was determined to confirm the membrane damage caused by MS-AgNPs. Membrane damage resulted in the release of cellular contents, such as nucleic acids and proteins, which were analyzed by the absorbance at 260 (Table 2) and 280 nm (Table 3). The bacterial cells treated with the MS-AgNPs and the bare AgNPs showed a significant difference compared to the antibiotic (ampicillin) and the control (Tables 2 and 3).

Table 2. OD at 260 nm of the cell constituent (nucleic acids) release from the selected bacterial strains upon treatment with MS-AgNPs, bare AgNPs, antibiotic, and control.

Bacterial Strains	MS-AgNPs (OD _{260 nm})	Bare AgNPs (OD _{260 nm})	Antibiotic (OD _{260 nm})	Control (OD _{260 nm})
<i>S. aureus</i>	0.26 ^a	0.22 ^b	0.14 ^c	0.006 ^d
<i>S. dysenteriae</i>	0.21 ^a	0.16 ^b	0.15 ^c	0.008 ^d
<i>S. typhi</i>	0.18 ^a	0.17 ^b	0.17 ^c	0.005 ^d

Different letters indicate significant differences at $p < 0.05$, determined by one-way ANOVA, within the same rows. The values are the mean of triplicate experiments.

Table 3. OD at 280 nm of the cell constituent (periplasmic proteins) release from the selected bacterial strains upon treatment with MS-AgNPs, bare AgNPs, antibiotic, and control.

Bacterial strains	MS-AgNPs (OD _{260 nm})	Bare AgNPs (OD _{260 nm})	Antibiotic (OD _{260 nm})	Control (OD _{260 nm})
<i>S. aureus</i>	0.32 ^a	0.21 ^b	0.11 ^c	0.003 ^d
<i>S. dysenteriae</i>	0.27 ^a	0.19 ^b	0.10 ^c	0.006 ^d
<i>S. typhi</i>	0.29 ^a	0.18 ^b	0.12 ^c	0.004 ^d

Different letters indicate significant differences at $p < 0.05$ by one-way ANOVA within the same rows. The values are the mean of triplicate experiments.

4. Discussion

Green chemistry and the manufacture of nanomaterials through biological resources is a fundamental approach to amalgamating nanotechnology and microbial biotechnology [13,49,50]. The catalytic potential of the microbes provides extraordinary opportunities to synthesize nanomaterials [51]. In this study, MS-Ag-NPs were synthesized for antimicrobial and biological applications. Ag-NPs exhibited color changes because of the excitation of surface plasmon vibration within the particles. The literature also supported the same method of biological synthesis of nano-sized Ag particles with diverse fungal strains [41,52]. Time is a major factor in completing the reaction. In the current study, 72 h were sufficient for incubation in the dark to obtain the desired results [42]. Moreover, varying the AgNO₃ concentration and reaction duration allowed for variations in color intensity because the MS-AgNPs showed dependent behavior on both factors throughout the synthetic procedures. The mechanism might involve electrostatic interactions between the ions of the Ag and the fungal macromolecules (peptides and proteins) released from the fungal extract. The precise mechanism regarding the interaction of biological compounds and Ag is not well understood. *Aspergillus* is the most extensively considered genus for the biogenic synthesis of nanoparticles with different metal oxides. Literature studies regarding *A. fumigatus* have explained that synthetic events of mycogenic Ag nanoparticles occur extracellularly [43]. An additional benefit of using fungus for this purpose is that fungal peptides and proteins, with the help of oxidoreductases and quinones, serve as metal scavengers during the detoxification procedures [44,45]. Similarly, an optimized incubation temperature (37 °C) plays a vital role in obtaining a huge AgNPs yield to maintain the lifeline of microbes. These findings showed that a higher AgNO₃ concentration (3 mM) is the optimum for MS-AgNPs. Moreover, the myco-synthesis of NPs is the latest and most stimulating area of research to overcome the need for antibacterial agents against

resistant bacterial strains. The broad peaks and intensity of the diffraction band indicate that the particles are crystalline and possess a smaller particle size. The obtained spectrum confirmed that the synthesized NPs are pure and possess a crystalline nature. The results confirmed that fungal metabolites played a significant role in the crystallization and nucleation of the particles [53]. The appearance of organic functional groups in the FTIR spectra confirmed the role of fungal metabolites in reducing the particle growth of MS-AgNPs. In addition, the presence of organic functional groups played a role in the synthesis of crystal size in MS-AgNPs. The existence of NH_2 and OH groups constrained the nuclear growth of Ag^+ , which assembled and reduced the core size NPs. These results proved that MS-AgNPs exhibit various organic functional groups that strengthen the efficiency of the MS-AgNPs in two ways: (i) the presence of an organic functional group helped to synthesize AgNPs that can be used in biological activities, and (ii) the fungal extract provides a surface for the AgNPs coated with biomolecules, which will facilitate the killing of pathogenic microorganisms. In UV analysis, the change in the color of the suspension from pale yellow to dark brown indicates the presence of Ag^+ ions in the solution. The maximum absorbance potential of the MS-AgNPs may be the result of the ionization of metabolites and organic compounds from the fungal extract. SEM images showed electrostatic interactions among the synthesized nanomaterial. The electrostatic interactions on the exterior surface of the NPs sheets might lead to the agglomeration of the AgNPs. On the other hand, the documented findings are in accordance with previously available research data [34]. The bacterium-killing capability of MS-AgNPs depends mainly on their spherical shape (morphology), which plays a vital role in synthetic pathways for its adsorption leading toward death [26]. The large surface area will facilitate the antimicrobial potential of the prepared AgNPs. Previous studies also showed the spherical shape of the AgNPs prepared with fungal extracts [17,21]. The difference in the antibacterial activity against different strains may be due to variations in the cell wall composition between Gram-positive and Gram-negative bacteria [54]. The cell walls of Gram-negative *S. dysenteriae* and *S. typhi* are surrounded by an outer lipopolysaccharide membrane that hinders particle attraction and penetration into the cells due to electrostatic repulsion between the NPs and bacterial strains [55]. Overall, the antibacterial potential of the MS-AgNPs was the highest compared to the other treatments [42]. MS-AgNPs could also penetrate the cellular components and damage the DNA, making it a suitable candidate for biomedicine in pharmaceuticals to overcome the resistance of microbes against antibiotics [56]. The mechanism of MS-AgNPs involves AgNPs liberating ions, which counter with sulfur-containing amino acids (thiol group) distributed on the exterior surface of the microbes. These amino acids are beneficial for the transportation of food materials through the microbial cell membrane. The presence of MS-AgNPs decreases the transportation of food across the membrane, which is entirely dependent on its permeability. In addition, it deactivates the protein, which finally caused the expiration of bacterial life [11]. The inhibition of bacterial cell division involves the effects of AgNPs on the synthesis of the bacterial cell membrane. Another reason for the inhibition of bacterial cell division is due to the prohibition of protein synthesis, damaging the DNA and metabolic pathways, leading to bacterial cell death [11,42]. The bacterial cell death is also due to hyperosmotic stress and imbalanced permeability resulting from the AgNPs. These results showed that the MS-AgNPs possess the highest antibacterial potential against resistant bacterial strains. The maximum effect of the MS-AgNPs on the surface of the bacterial membrane may be attributed to the electrostatic interaction of the MS-AgNPs and the bacterial cell surface. These results agree with previous studies showing surface damage of the bacterial membrane with an NP treatment [9,47]. These results suggest that changes in the surface potential values after treatment with NPs may be due to the release of cellular contents, which leads to bacterial membrane damage [29]. Therefore, it is necessary to evaluate the effect of the synthesized MS-AgNPs on the release of the cellular contents. The MS-AgNPs showed the maximum effect on *S. aureus*, which also suggests that the prepared NPs significantly influence the bacterial growth of Gram-positive bacteria. Moreover, the MS-AgNPs also influenced the cellular contents

of *S. dysenteriae* and *S. typhi*. The improved activity of the MS-AgNPs can be assigned to interactions of the NPs with the bacterial cell surface [11,35].

5. Conclusions

The findings of this study recommended that crystalline and stable nanomaterials can be manufactured through the application of fungal strains. Our study showed that the MS-AgNPs and the bare AgNPs represent the face-centered cubic structure of AgNPs. The fungal metabolites (hydroxyl stretch coupled with carbonyl group) resulting from a fungal extract played a key role in reducing and stabilizing the NPs. The MS-AgNPs exhibit the potential to inhibit bacterial growth by damaging the cell membrane, causing the release of cellular contents. Our study suggests that changes in the bacterial cell membrane surface occur after treatment with the NPs due to the release of cellular contents, which leads to bacterial membrane damage and cell death. The antibacterial potential of the MS-AgNPs was significantly increased by the presence of functional groups from *A. fumigatus*. Therefore, it is recommended that applications of microbes in the synthesis process of NPs can facilitate the synthesis of NPs effective for the inhibition of various pathogenic bacterial strains.

Author Contributions: W.Z., S.F., B.A. and S.S. wrote the manuscript; M.I.A., M.Y., M.N. (Muhammad Naeem) and W.Z. designed the experiments; M.N. (Momina Nisar), F.U., M.I.A. and S.S. analyzed the data and helped in characterizations; M.Y., S.A., A.M.E., A.S., T.K.Z.E.-A., H.O.E. and M.I.A. revised the manuscript and helped with the experiments. All authors have read and agreed to the published version of the manuscript.

Funding: This research was funded by King Saud University (RSP-2021/56).

Institutional Review Board Statement: Not applicable.

Informed Consent Statement: Not applicable.

Data Availability Statement: All data analyzed and generated in this study are included in this manuscript.

Acknowledgments: The authors extend their deep appreciation to the Researchers Supporting Project number (RSP-2021/56), King Saud University, Riyadh, Saudi Arabia. We are thankful to the Department of Biotechnology, Mohi-ud-din Islamic University, Nerian Sahreef, AJ&K, Pakistan, and the Medical College, Mohi-ud-din Islamic University, Mirpur, AJ&K, Pakistan, for providing basic lab facilities during the experiments.

Conflicts of Interest: The authors declare no conflict of interest.

References

1. Regiel-Futyra, A.; Dąbrowski, J.M.; Mazuryk, O.; Śpiewak, K.; Kyzioł, A.; Pucelik, B.; Brindell, M.; Stochel, G. Bioinorganic antimicrobial strategies in the resistance era. *Coord. Chem. Rev.* **2017**, *351*, 76–117. [[CrossRef](#)]
2. Afewerki, S.; Bassous, N.; Harb, S.; Palo-Nieto, C.; Ruiz-Esparza, G.U.; Marciano, F.R.; Webster, T.J.; Furtado, A.S.A.; Lobo, A.O. Advances in dual functional antimicrobial and osteoinductive biomaterials for orthopaedic applications. *Nanomed. Nanotechnol. Biol. Med.* **2020**, *24*, 102143. [[CrossRef](#)] [[PubMed](#)]
3. Khan, I.; Saeed, K.; Khan, I. Nanoparticles: Properties, applications and toxicities. *Arab. J. Chem.* **2019**, *12*, 908–931. [[CrossRef](#)]
4. Chand, K.; Cao, D.; Fouad, D.E.; Shah, A.H.; Dayo, A.Q.; Zhu, K.; Lakhan, M.N.; Mehdi, G.; Dong, S. Green synthesis, characterization and photocatalytic application of silver nanoparticles synthesized by various plant extracts. *Arab. J. Chem.* **2020**, *13*, 8248–8261. [[CrossRef](#)]
5. Mohanta, Y.K.; Panda, S.K.; Bastia, A.K.; Mohanta, T.K. Biosynthesis of silver nanoparticles from *Protium serratum* and investigation of their potential impacts on food safety and control. *Front. Microbiol.* **2017**, *8*, 626. [[CrossRef](#)]
6. Saqib, S.; Zaman, W.; Ullah, F.; Majeed, I.; Ayaz, A.; Hussain Munis, M.F. Organometallic assembling of chitosan-Iron oxide nanoparticles with their antifungal evaluation against *Rhizopus oryzae*. *Appl. Organomet. Chem.* **2019**, *33*, e5190. [[CrossRef](#)]
7. Sunera, A.; Saqib, S.; Uddin, S.; Zaman, W.; Ullah, F.; Ayaz, A.; Asghar, M.; Rehman, S.; Munis, M.; Chaudhary, H. Characterization and phytostimulatory activity of bacteria isolated from tomato (*Lycopersicon esculentum* Mill.) rhizosphere. *Microb. Pathog.* **2020**, *140*, 103966. [[CrossRef](#)] [[PubMed](#)]

8. Grün, A.Y.; App, C.B.; Breidenbach, A.; Meier, J.; Metreveli, G.; Schaumann, G.E.; Manz, W. Effects of low dose silver nanoparticle treatment on the structure and community composition of bacterial freshwater biofilms. *PLoS ONE* **2018**, *13*, e0199132. [[CrossRef](#)] [[PubMed](#)]
9. Asghar, M.; Habib, S.; Zaman, W.; Hussain, S.; Ali, H.; Saqib, S. Synthesis and characterization of microbial mediated cadmium oxide nanoparticles. *Microsc. Res. Tech.* **2020**, *83*, 1574–1584. [[CrossRef](#)]
10. Bocate, K.P.; Reis, G.F.; de Souza, P.C.; Junior, A.G.O.; Durán, N.; Nakazato, G.; Furlaneto, M.C.; de Almeida, R.S.; Panagio, L.A. Antifungal activity of silver nanoparticles and simvastatin against toxigenic species of *Aspergillus*. *Int. J. Food Microbiol.* **2019**, *291*, 79–86. [[CrossRef](#)]
11. Azam, Z.; Ayaz, A.; Younas, M.; Qureshi, Z.; Arshad, B.; Zaman, W.; Ullah, F.; Nasar, M.Q.; Bahadur, S.; Irfan, M.M. Microbial synthesized cadmium oxide nanoparticles induce oxidative stress and protein leakage in bacterial cells. *Microb. Pathog.* **2020**, *144*, 104188. [[CrossRef](#)] [[PubMed](#)]
12. Gopinath, V.; MubarakAli, D.; Vadivelu, J.; Kamath, S.M.; Syed, A.; Elgorban, A.M. Synthesis of biocompatible chitosan decorated silver nanoparticles biocomposites for enhanced antimicrobial and anticancer property. *Process Biochem.* **2020**, *99*, 348–356. [[CrossRef](#)]
13. Saleh, H.E.-D.M.; Koller, M. Introductory chapter: Principles of green chemistry. In *Green Chemistry*; IntechOpen: London, UK, 2018.
14. Hu, X.; Saravanakumar, K.; Jin, T.; Wang, M.-H. Mycosynthesis, characterization, anticancer and antibacterial activity of silver nanoparticles from endophytic fungus *Talaromyces purpureogenus*. *Int. J. Nanomed.* **2019**, *14*, 3427. [[CrossRef](#)]
15. Prabakaran, K.; Ragavendran, C.; Natarajan, D. Mycosynthesis of silver nanoparticles from *Beauveria bassiana* and its larvicidal, antibacterial, and cytotoxic effect on human cervical cancer (HeLa) cells. *RSC Adv.* **2016**, *6*, 44972–44986. [[CrossRef](#)]
16. Asghar, M.; Younas, M.; Arshad, B.; Zaman, W.; Ayaz, A.; Rasheed, S.; Shah, A.H.; Ullah, F.; Saqib, S. Bioactive potential of cultivated *Mentha arvensis* L. For preservation and production of health-oriented food. *J. Anim. Plant Sci.* **2022**, *32*, 835–844.
17. Deplanche, K.; Merroun, M.L.; Casadesus, M.; Tran, D.T.; Mikheenko, I.P.; Bennett, J.A.; Zhu, J.; Jones, I.P.; Attard, G.A.; Wood, J. Microbial synthesis of core/shell gold/palladium nanoparticles for applications in green chemistry. *J. R. Soc. Interface* **2012**, *9*, 1705–1712. [[CrossRef](#)] [[PubMed](#)]
18. Raftery, R.M.; Tierney, E.G.; Curtin, C.M.; Cryan, S.-A.; O'Brien, F.J. Development of a gene-activated scaffold platform for tissue engineering applications using chitosan-pDNA nanoparticles on collagen-based scaffolds. *J. Control. Release* **2015**, *210*, 84–94. [[CrossRef](#)] [[PubMed](#)]
19. Dos Santos, C.A.; Seckler, M.M.; Ingle, A.P.; Gupta, I.; Galdiero, S.; Galdiero, M.; Gade, A.; Rai, M. Silver nanoparticles: Therapeutic uses, toxicity, and safety issues. *J. Pharm. Sci.* **2014**, *103*, 1931–1944. [[CrossRef](#)] [[PubMed](#)]
20. Omran, B.A. Versatile Applications of Biosynthesized Nanoparticles, Global Safety Issues, Grand Challenges, and Future Perspectives Regarding Nanobiotechnology. In *Nanobiotechnology: A Multidisciplinary Field of Science*; Springer: Berlin/Heidelberg, Germany, 2020; pp. 185–221.
21. Guilger-Casagrande, M.; de Lima, R. Synthesis of silver nanoparticles mediated by fungi: A Review. *Front. Bioeng. Biotechnol.* **2019**, *7*, 287. [[CrossRef](#)] [[PubMed](#)]
22. Shahzad, A.; Iqtedar, M.; Saeed, H.; Hussain, S.Z.; Chaudhary, A.; Abdullah, R.; Kaleem, A. Mycosynthesis of size-controlled silver nanoparticles through optimization of process variables by response surface methodology. *Pol. J. Microbiol.* **2019**, *68*, 35–42. [[CrossRef](#)] [[PubMed](#)]
23. Liaquat, F.; Munis, M.F.H.; Haroon, U.; Arif, S.; Saqib, S.; Zaman, W.; Khan, A.R.; Shi, J.; Che, S.; Liu, Q. Evaluation of metal tolerance of fungal strains isolated from contaminated mining soil of Nanjing, China. *Biology* **2020**, *9*, 469. [[CrossRef](#)] [[PubMed](#)]
24. Palomo, J.M.; Filice, M. Biosynthesis of metal nanoparticles: Novel efficient heterogeneous nanocatalysts. *Nanomaterials* **2016**, *6*, 84. [[CrossRef](#)] [[PubMed](#)]
25. Akhtar, M.S.; Swamy, M.K.; Sinniah, U.R. *Natural Bio-Active Compounds: Volume 1: Production and Applications*; Springer Nature: London, UK, 2019.
26. Saqib, S.; Nazeer, A.; Ali, M.; Zaman, W.; Younas, M.; Shahzad, A.; Nisar, M. Catalytic potential of endophytes facilitates synthesis of biometallic zinc oxide nanoparticles for agricultural application. *BioMetals* **2022**, 1–19. [[CrossRef](#)] [[PubMed](#)]
27. Madakka, M.; Jayaraju, N.; Rajesh, N. Mycosynthesis of silver nanoparticles and their characterization. *MethodsX* **2018**, *5*, 20–29. [[CrossRef](#)]
28. Liaquat, F.; Munis, M.F.H.; Arif, S.; Haroon, U.; Shi, J.; Saqib, S.; Zaman, W.; Che, S.; Liu, Q. PacBio single-molecule long-read sequencing reveals genes tolerating manganese stress in *Schima superba* saplings. *Front. Genet.* **2021**, *12*, 635043. [[CrossRef](#)] [[PubMed](#)]
29. Khan, A.U.; Malik, N.; Khan, M.; Cho, M.H.; Khan, M.M. Fungi-assisted silver nanoparticle synthesis and their applications. *Bioprocess Biosyst. Eng.* **2018**, *41*, 1–20. [[CrossRef](#)] [[PubMed](#)]
30. Jampilek, J.; Kralova, K. Advances in Biologically Applicable Graphene-Based 2D Nanomaterials. *Int. J. Mol. Sci.* **2022**, *23*, 6253. [[CrossRef](#)] [[PubMed](#)]
31. El-Bendary, M.A.; Moharam, M.E.; Hamed, S.R.; Abo El-Ola, S.M.; Khalil, S.K.; Mounier, M.M.; Roshdy, A.M.; Allam, M.A. Mycosynthesis of silver nanoparticles using *Aspergillus caespitosus*: Characterization, antimicrobial activities, cytotoxicity, and their performance as an antimicrobial agent for textile materials. *Appl. Organomet. Chem.* **2021**, *35*, e6338. [[CrossRef](#)]

32. Peters, R.J.; Bouwmeester, H.; Gottardo, S.; Amenta, V.; Arena, M.; Brandhoff, P.; Marvin, H.J.; Mech, A.; Moniz, F.B.; Pesudo, L.Q. Nanomaterials for products and application in agriculture, feed and food. *Trends Food Sci. Technol.* **2016**, *54*, 155–164. [[CrossRef](#)]
33. Sharma, R.; Dewanjee, S.; Kole, C. Utilization of nanoparticles for plant protection. In *Plant Nanotechnology*; Springer: Berlin/Heidelberg, Germany, 2016; pp. 305–327.
34. Bala, M.; Arya, V. Biological synthesis of silver nanoparticles from aqueous extract of endophytic fungus *Aspergillus Fumigatus* and its antibacterial action. *Int. J. Nanomater. Biostructures* **2013**, *3*, 37–41.
35. Rafique, M.; Sadaf, I.; Rafique, M.S.; Tahir, M.B. A review on green synthesis of silver nanoparticles and their applications. *Artif. Cells Nanomed. Biotechnol.* **2017**, *45*, 1272–1291. [[CrossRef](#)]
36. Gupta, M.; Shukla, K.K. Endophytic Fungi: A Treasure Trove of Novel Bioactive Compounds. In *Bioactive Natural Products in Drug Discovery*; Springer: Berlin/Heidelberg, Germany, 2020; pp. 427–449.
37. Das, S.K.; Mahapatra, S. Isolation and Characterization of Bioactive Compound from Endophytic Fungus of Spoiled Fruits. *Int. J. Res. Anal. Rev.* **2019**, *7*, 65–72.
38. Jyoti, K.; Baunthiyal, M.; Singh, A. Characterization of silver nanoparticles synthesized using *Urtica dioica* Linn. leaves and their synergistic effects with antibiotics. *J. Radiat. Res. Appl. Sci.* **2016**, *9*, 217–227. [[CrossRef](#)]
39. Salleh, A.; Naomi, R.; Utami, N.D.; Mohammad, A.W.; Mahmoudi, E.; Mustafa, N.; Fauzi, M.B. The potential of silver nanoparticles for antiviral and antibacterial applications: A mechanism of action. *Nanomaterials* **2020**, *10*, 1566. [[CrossRef](#)] [[PubMed](#)]
40. Fang, J.; Zhong, C.; Mu, R. The study of deposited silver particulate films by simple method for efficient SERS. *Chem. Phys. Lett.* **2005**, *401*, 271–275. [[CrossRef](#)]
41. Feroze, N.; Arshad, B.; Younas, M.; Afridi, M.I.; Saqib, S.; Ayaz, A. Fungal mediated synthesis of silver nanoparticles and evaluation of antibacterial activity. *Microsc. Res. Tech.* **2020**, *83*, 72–80. [[CrossRef](#)]
42. Ramesh, P.; Kokila, T.; Geetha, D. Plant mediated green synthesis and antibacterial activity of silver nanoparticles using *Emblca officinalis* fruit extract. *Spectrochim. Acta Part A Mol. Biomol. Spectrosc.* **2015**, *142*, 339–343. [[CrossRef](#)] [[PubMed](#)]
43. Magdi, H.M.; Mourad, M.H.; El-Aziz, M. Biosynthesis of silver nanoparticles using fungi and biological evaluation of mycosynthesized silver nanoparticles. *Egypt J. Exp. Biol.* **2014**, *10*, 1–12.
44. Alawfi, A.A.; Henari, F.Z.; Younis, A.; Manaa, H. Bio-inspired synthesis of silver nanoparticles using *Hibiscus Tiliaceus* L. flower extracts for improved optical characteristics. *J. Mater. Sci. Mater. Electron.* **2020**, *31*, 21073–21081. [[CrossRef](#)]
45. Tyagi, S.; Tyagi, P.K.; Gola, D.; Chauhan, N.; Bharti, R.K. Extracellular synthesis of silver nanoparticles using entomopathogenic fungus: Characterization and antibacterial potential. *SN Appl. Sci.* **2019**, *1*, 1545. [[CrossRef](#)]
46. Siddiqi, K.S.; Husen, A.; Rao, R.A. A review on biosynthesis of silver nanoparticles and their biocidal properties. *J. Nanobiotechnology* **2018**, *16*, 14. [[CrossRef](#)]
47. Besinis, A.; Hadi, S. d.; Le, H.; Tredwin, C.; Handy, R. Antibacterial activity and biofilm inhibition by surface modified titanium alloy medical implants following application of silver, titanium dioxide and hydroxyapatite nanocoatings. *Nanotoxicology* **2017**, *11*, 327–338. [[CrossRef](#)] [[PubMed](#)]
48. Nithya, R.; Raganathan, R. Synthesis of silver nanoparticle using *Pleurotus sajor caju* and its antimicrobial study. *Dig. J. Nanomater. Biostructures* **2009**, *4*, 623–629.
49. Kalia, S.; Kaith, B.; Kaur, I. *Cellulose Fibers: Bio-and Nano-Polymer Composites: Green Chemistry and Technology*; Springer Science & Business Media: Berlin, Germany, 2011.
50. Das, R.K.; Brar, S.K. Plant mediated green synthesis: Modified approaches. *Nanoscale* **2013**, *5*, 10155–10162. [[CrossRef](#)] [[PubMed](#)]
51. Saadat, S.; Pandey, G.; Tharmavaram, M.; Braganza, V.; Rawtani, D. Nano-interfacial decoration of Halloysite Nanotubes for the development of antimicrobial nanocomposites. *Adv. Colloid Interface Sci.* **2020**, *275*, 102063. [[CrossRef](#)]
52. Sarsar, V.; Selwal, M.K.; Selwal, K.K. Biofabrication, characterization and antibacterial efficacy of extracellular silver nanoparticles using novel fungal strain of *Penicillium atramentosum* KM. *J. Saudi Chem. Soc.* **2015**, *19*, 682–688. [[CrossRef](#)]
53. Khatami, M.; Varma, R.S.; Zafarnia, N.; Yaghoobi, H.; Sarani, M.; Kumar, V.G. Applications of green synthesized Ag, ZnO and Ag/ZnO nanoparticles for making clinical antimicrobial wound-healing bandages. *Sustain. Chem. Pharm.* **2018**, *10*, 9–15. [[CrossRef](#)]
54. Taglietti, A.; Diaz Fernandez, Y.A.; Amato, E.; Cucca, L.; Dacarro, G.; Grisoli, P.; Necchi, V.; Pallavicini, P.; Pasotti, L.; Patrini, M. Antibacterial activity of glutathione-coated silver nanoparticles against gram positive and gram negative bacteria. *Langmuir* **2012**, *28*, 8140–8148. [[CrossRef](#)]
55. Dey, A.; Pandey, G.; Rawtani, D. Functionalized nanomaterials driven antimicrobial food packaging: A technological advancement in food science. *Food Control* **2022**, *131*, 108469. [[CrossRef](#)]
56. Abdel-Hafez, S.I.; Nafady, N.A.; Abdel-Rahim, I.R.; Shaltout, A.M.; Daròs, J.-A.; Mohamed, M.A. Assessment of protein silver nanoparticles toxicity against pathogenic *Alternaria solani*. *3 Biotech* **2016**, *6*, 199. [[CrossRef](#)]